American Journal of Ophthalmology Case Reports 28 (2022) 101706

Contents lists available at ScienceDirect

American Journal of Ophthalmology Case Reports

journal homepage: www.ajocasereports.com/

Microstructural changes of photoreceptor layers detected by ultrahigh-resolution SD-OCT in patients with autosomal recessive bestrophinopathy

Kazushige Tsunoda [a,*], Gen Hanazono [a,b]

[a] Division of Vision Research, National Institute of Sensory Organs, National Hospital Organization Tokyo Medical Center, Tokyo, Japan
[b] Higashimatsudo Hanazono Eye Clinic, Chiba, Japan

ARTICLE INFO

Keywords:
Autosomal recessive bestrophinopathy
BEST1
Interdigitation zone
Ellipsoid zone
Photoreceptor
Spectral-domain OCT
Ultrahigh-resolution OCT

ABSTRACT

Purpose: To determine the changes in the microstructures of the photoreceptors in patients with autosomal recessive bestrophinopathy (ARB) by ultrahigh-resolution spectral-domain optical coherence tomography (UHR-SD-OCT).

Methods: Five eyes of 4 patients with ARB were studied. Cross-sectional images of the fovea were recorded by the UHR-SD-OCT system with a depth resolution of <2.0 μm.

Results: The UHR-SD-OCT images revealed changes in the outer retinal structures that were dependent on the severity of the photoreceptor atrophy. There was an increase in the reflectivity and appearance of small hyperreflective dots (HRDs) in the outer segments, followed by an irregularity and decrease in the length of the outer segments, then a disruption of the ellipsoid zone (EZ) band, and appearance of large HRDs corresponding to the segmented ellipsoids. Finally, there was a disappearance of the large HRDs followed by a localized thinning of the outer nuclear layer and appearance of hyperreflective foci above the region of the disrupted EZ.

Conclusions: UHR-SD-OCT can record images that show detailed changes of the microstructures of the photoreceptors at different stages of ARB. These observations should help in determining the mechanisms involved in retinal pathology and should provide important information on the effectiveness of treatments.

1. Introduction

Autosomal recessive bestrophinopathy (ARB; OMIM-611809) is one of the BEST1-related retinopathies that is caused by biallelic pathogenic variants of the *BEST1* gene.[1,2] ARB shares common clinical features with Best vitelliform macular dystrophy (VMD; OMIM-153700), which is caused by a single pathogenic variant of the *BEST1* gene.[1–3] The retinal structural changes of ARB have been described from the spectral-domain optical coherence tomographic (SD-OCT) images,[4–6] and these features are essentially the same as those in cases of VMD.[3,7–12] However, due to the limited axial resolution of the conventional SD-OCT, there is a significant gap in what is observed in the diseased retina by the conventional OCT and what is happening structurally during the process of neuronal atrophy of the retinas. The findings made from the conventional SD-OCT images from eyes with both VMD and ARB partially corresponded with the histological studies of postmortem eyes with VMD.[13–17] However, histological studies cannot determine the structural changes of the photoreceptor layer in VMD and ARB in detail because of the fragility of the photoreceptor cells to histological processing.

An ultrahigh-resolution SD-OCT (UHR-SD-OCT; KOWA OCT Bi-μ; Kowa Company, Ltd., Japan) device has become available which has an axial resolution of <2.0 μm which is about three-times better than the conventional SD-OCT. It can obtain clearer images of the outer retinal structures both in normal[18,19] and diseased eyes.[20–22] Matsui et al. presented a B-scan image of a patient with ARB obtained by the UHR-SD OCT and showed detailed structural changes which could not be observed by the conventional SD-OCT devices.[18] We have examined the microstructures of the photoreceptor layer in eyes with occult macular dystrophy (OMD, Miyake's disease) by UHR-SD-OCT and were able to determine the characteristics of the photoreceptor microstructures at different stages of OMD.[22]

* Corresponding author. Division of Vision Research, National Institute of Sensory Organs, National Hospital Organization Tokyo Medical Center, 2-5-1 Higashigaoka, Meguro-ku, Tokyo, 152-8902, Japan.
E-mail address: kazushige.tsunoda@kankakuki.jp (K. Tsunoda).

https://doi.org/10.1016/j.ajoc.2022.101706
Received 21 May 2022; Received in revised form 2 September 2022; Accepted 9 September 2022
Available online 24 September 2022

The purpose of this study was to determine the changes in the microstructures of the photoreceptors in eyes with ARB. To accomplish this, we examined the B-scan images obtained by the UHR-SD-OCT of 5 eyes of 4 patients with ARB of the same genotypes but of different severities. Our findings will fill the gap between the OCT images and the histological findings in eyes with ARB which should help in determining the mechanisms for the degeneration of the photoreceptors.

2. Patients and methods

The procedures used in this study adhered to the tenets of the Declaration of Helsinki and were approved by the Ethics Committee of the National Institute of Sensory Organs, National Hospital Organization Tokyo Medical Center (Reference, R18-029). A signed informed consent was received from all subjects for the examinations after an explanation of the nature and possible consequences of the study.

2.1. Participants

We examined 5 eyes of 4 unrelated patients with ARB. The phenotype of these patients was determined by comprehensive ophthalmic examinations including ophthalmoscopy, fundus photography, fundus autofluorescence (FAF; HRA 2; excitation light, 488 nm; barrier filter, 500 nm; Heidelberg Engineering, Heidelberg, Germany), conventional SD-OCT (Cirrus HD OCT, version 6.5; Carl Zeiss Meditec, Dublin, CA, USA), electrooculography (SG-2002, LKC Technologies, Gaithersburg, MD, USA), and full-field electroretinography (ERG; LE4000, Tomey Corporation, Aichi, Japan).[23] For the recording by the conventional OCT, we used the 'HD 5 Line Raster' mode, and averaged four 9.0 mm B-scan images to obtain one averaged B-scan image. Genetic analysis was performed on all the patients. To search for the causative genes, whole exome sequencing with targeted analysis for retinal disease-causing genes on RetNET (https://sph.uth.edu/retnet/home.htm) and inheritance filtration were performed as described in detail.[4,24] The details of the whole exome sequencing and in silico molecular genetic analyses are described as supplemental information (**Supplementary Methods for the Genetic Analysis**). All 4 cases of ARB had the same compound heterozygous pathogenic variants of the *BEST1* gene (c.584C > T, p.Ala195Val; c.763C > T, p.Arg255Trp: mRNA reference sequence, NM_004183.3).[25]

2.2. UHR-SD-OCT imaging

An UHR-SD-OCT system (KOWA OCT Bi-μ; Kowa Company, Ltd., Japan) with a broadband superluminescent diode was used on all subjects.[18,19,22] The center wavelength of the light source was 860 nm, and the bandwidth was 135 nm. Each A-scan had a depth of 2.6 mm which was comprised of 2048 pixels and allowed a digital depth sampling of 1.27 μm/pixel. Each B-scan spanned 30° and consisted of 1800 A-scans. For a 9.0 mm width image, the digital width sampling was 5 μm/pixel. A detailed technical description of this imaging device has been published elsewhere.[18,19] Cross-sectional horizontal and vertical images with a 9.0 mm width across the fovea were recorded in all the subjects with dilated pupils. The original averaging technique of 'A-scan matching algorithm' was taken to improve the clarity of the OCT images, and the procedures were described in detail elsewhere.[18,19] Briefly, twenty B-scans images which had higher correlation coefficients to the base image were chosen from the fifty B-scan images, and averaged for the final B scan image. The examination required a fixation of 1.5 s to obtain a horizontal B-scan image from either a normal or diseased eye.

3. Results

3.1. UHR-SD-OCT images of normal eyes

The phenotypic and genotypic findings of the four cases are

Table 1
Summary of four cases with autosomal recessive bestrophinopathy.

Case ID	OD/OS	Age at Examination	Sex	Symptoms at Onset	Age of Onset	BCVA	OCT Findings of the Macula						Nucleotide Changes of *BEST1* Gene	Amino Acid Changes
							SRF	Elongation of OS	Atrophy of OS	Disruption of EZ	Abnormality of ONL	Focal Choroidal Excavation		
1	OD (Figs. 2A and 3A)	33	F	No symptom	No symptom	20/20	+	+	–	–	–	–	c.584C > T, c.763C > T	p.A195V, p.R255W
	OS (Figs. 2E and 3E)					20/20	+	+	+	+	+	+		
2	OD	20	F	No symptom	No symptom	20/20	+	+	±	–	–	+	c.584C > T, c.763C > T	p.A195V, p.R255W
	OS (Figs. 2B and 3B)					20/20	+	+	±	–	–	–		
3	OD	36	F	Reduced visual acuity (OD)	32	20/25	+	+	+	+	–	+	c.584C > T, c.763C > T	p.A195V, p.R255W
	OS (Figs. 2C and 3C)					20/20	+	+	+	+	–	+		
4	OD (Figs. 2D and 3D)	55	M	Reduced visual acuity (OD)	49	20/125	+	–	+	+	–	–	c.584C > T, c.763C > T	p.A195V, p.R255W
	OS					20/25	+	+	±	–	–	–		

OD = right eye; OS = left eye; BCVA = best corrected visual acuity; OCT = optical coherence tomography; SRF = subretinal fluid; OS = outer segment; EZ = ellipsoid zone; ONL = outer nuclear layer.

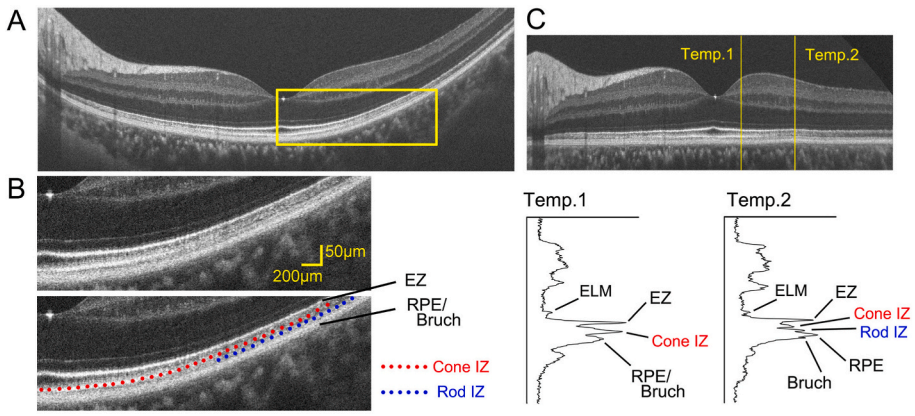

Fig. 1. Ultrahigh-resolution spectral domain optical coherence tomorgraphic (UHR-SD-OCT) images of a normal eye. **A.** Horizontal B-scan image across the fovea of a normal eye of a 41-year-old woman eye taken by a UHR-SDR-OCT device. **B.** Expanded image of the yellow rectangle in **A**. The locations of both the cone IZ and rod IZ are shown by red and blue dotted lines, respectively. **C.** Longitudinal reflectivity profiles (LRP) in the regions indicated by yellow arrows on the flattened OCT image. The rod IZ is seen as a distinct hyperreflective peak between the cone IZ and RPE/Bruch's membrane in Temp. 2 but not in Temp.1. EZ = ellipsoid zone of photoreceptor; IZ = interdigitation zone of photoreceptor; RPE = retinal pigment epithelium. (For interpretation of the references to colour in this figure legend, the reader is referred to the Web version of this article.)

presented in Table 1. Representative horizontal B-scan images across the fovea of the normal eye of a 41-year-old woman taken with the UHR-SDR-OCT device are presented in Fig. 1A and B together with the longitudinal reflectivity profiles (LRP; Fig. 1C). Hyperreflective regions were present which were not mentioned in the International Nomenclature for Optical Coherence Tomography [IN•OCT],[26] viz., a rod IZ and Bruch's membrane.

3.2. UHR SD-OCT images of eyes with ARB

Fundus photographs and FAF images of the 5 eyes of 4 cases with ARB are shown in Fig. 2. All of the cases were bilateral, and the funduscopic changes corresponded approximately with those of eyes with VMD at the vitelliruptive or scrambled-egg stage.[3] The FAF images showed hyper autofluorescence (AF) spots in Cases A, B, D, and E, or a hyper AF ring at the border of the affected region in Case C. The macular region showed hypo AF in all cases. In Cases B, C, and D, the affected region extended beyond the macula which is typical of cases with ARB.[3–5]

The conventional SD-OCT images showed that these eyes had characteristic structural changes that are typical of that between the pseudohypopyon and vitelliruptive stages, viz, subretinal fluid (SRF) in the macula, absence of the IZ, elongation of the photoreceptor outer segments, disruption of the EZ, and focal choroidal excavation (Fig. 3F).[4–6,8,10,11]

The UHR-SD-OCT B-scan images of the five eyes with ARB (Fig. 2) are shown in Fig. 3. Cases A to E are aligned according to the severity of the photoreceptor damage from mild to severe. One B-scan image of the same eye as in Fig. 3A taken by a conventional SD-OCT is shown for comparison (Fig. 3F). Further expanded images (x 2.5) of the outer segment regions in the right column in **Figures A, F, and B** are shown in Fig. 3G.

The OCT images of the right eye of a 33-year-old woman whose best-corrected visual acuity (BCVA) was 20/20 are shown in Fig. 3A. There is a shallow retinal detachment in the peri-macular region (Fig. 3A, white arrow), where the cone IZ is not present and the outer segments are elongated and hyperreflective. Part of the outer segments in the detached region resembled icicles hanging on the EZ (Fig. 3A and G left, asterisk).

The OCT images of the left eye of a 20-year-old woman whose BCVA was 20/20 are shown in Fig. 3B. Similar to the earlier case, the outer segments are elongated and hyperreflective material that resembled icicles can be seen hanging on the EZ (Fig. 3B and G right, asterisk). The peripheral edge of the outer segments was irregularly aligned, and the cone IZ was not observed in the detached region. There were debris-like hyperreflective spots between the outer segments and the RPE (Fig. 3B, double asterisks).

The OCT images of the left eye of a 36-year-old woman whose BCVA was 20/20 are shown in Fig. 3C. The outer segments are shortened and the EZ band is disrupted and composed of individual large hyperreflective dots (HRDs; Fig. 3C, yellow arrowheads). These HRDs were connected to the ELM with a less highly reflective bridge-like structures. The outer segments could not be clearly seen. Instead, thin icicle-like structures could be seen hanging on the ELM (Fig. 3C, yellow asterisks).

The OCT images of the right eye of a 55-year-old man whose BCVA was 20/125 due to the loss of photoreceptors at the fovea are shown in Fig. 3D. The EZ band was disrupted and a small number of large HRDs was seen connected to the ELM (Fig. 3D, yellow arrowheads). Thin icicle-like structures can be seen hanging directly on the ELM (Fig. 3D, yellow asterisks).

The OCT images of the right eye of the patient shown in Fig. 3A whose BCVA was 20/20 are shown in Fig. 3E. The expanded image shows a widely disrupted EZ with preserved ELM inferior to the fovea (Fig. 3E, white arrowhead). At the location of the disrupted EZ, the outer nuclear layer (ONL) is thin (Fig. 3E, white arrowhead). There are hyperreflective spots scattered in the ONL above the disrupted EZ (Fig. 3E, white arrowhead), which are known as hyperreflective foci (HRF).[9,27]

4. Discussion

4.1. Process of photoreceptor atrophy in eyes with ARB

This was an observational study of 5 eyes of 4 unrelated individuals with ARB, and we assumed that there was a longitudinal progression of the disease process that could be determined by the cross-sectional observations of the cases with different severities but with the same genotype. The early abnormality of the photoreceptor layer was observed in the perimacular region as a shallow SRF lesion in the UHR-SD-OCT images (Fig. 3A, white arrow). The cone IZ became indistinct and disappeared, and the outer segments became hyperreflective and elongated with small HRDs aligned in a row like icicles or string of pearls hanging on the EZ (Fig. 3A, asterisk and Fig. 3G, left). In the macular region with a larger SRF, the peripheral edges of the outer segments were irregularly aligned (Fig. 3B, asterisks and Fig. 3G, right) and some parts of the icicle-like outer segments appeared to be shortened with debris-like hyperreflective spots in the SRF (Fig. 3B, double asterisks). In addition, the EZ band became disrupted and was seen as large HRDs connected to the ELM with less highly reflective bridge-like structures (Fig. 3C and D, yellow arrowheads). In the next stage, the disrupted EZ was more atrophic, and the large HRDs were replaced by thin string-like icicles hanging directly on the ELM (Fig. 3D, yellow asterisks). During these processes, the ONL become thinner (Fig. 3C and D), and the outer plexiform layer appeared to be closer to the ELM with scattered HRF above the disrupted EZ in the region where icicle-like formation was completely lost (Fig. 3E, white arrowhead).These HRF could also be

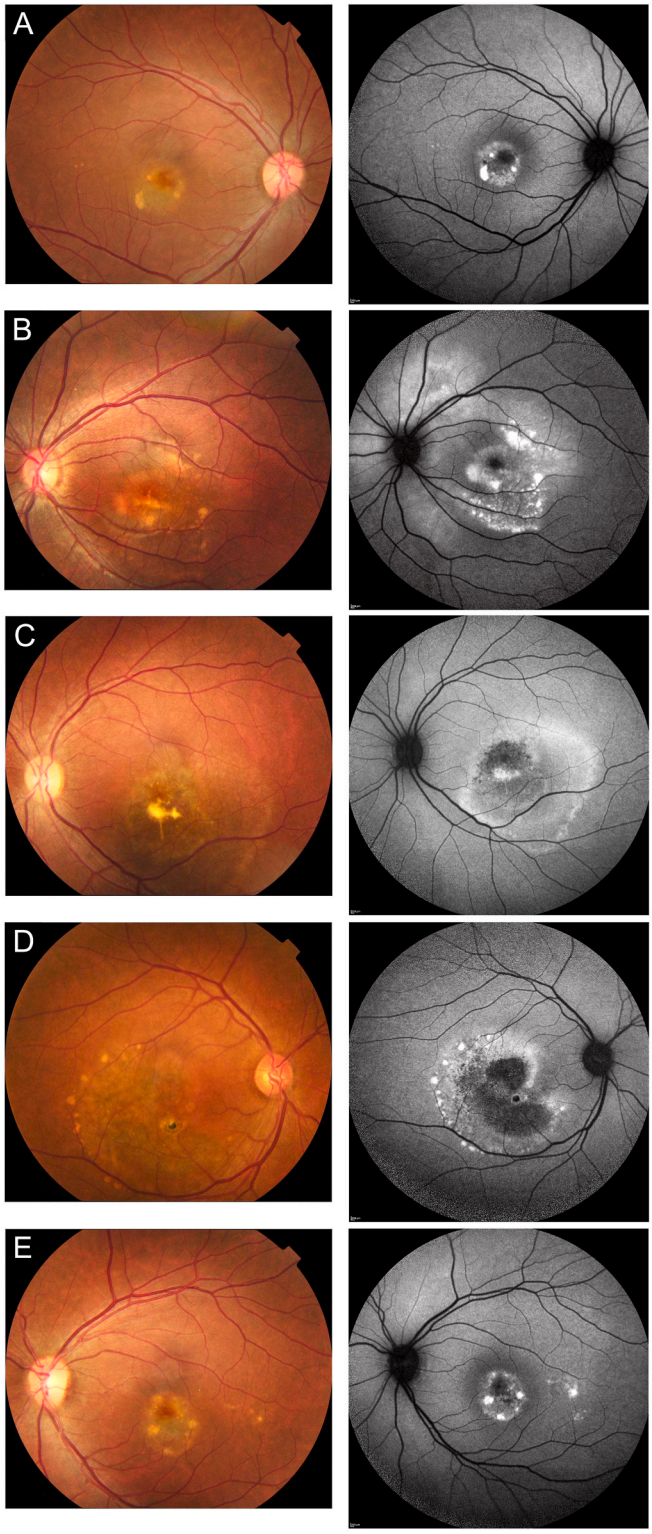

Fig. 2. Fundus photographs and fundus autofluorescence (FAF) images of the retina of eyes with autosomal recessive bestrophinopathy (ARB). Fundus photographs (left column) and FAF images (right column) of the five eyes of four cases with ARB are shown. The images in **E** show the left eye of the patient in **A**.

observed in the conventional OCT images.[9,27] These characteristic features in eyes with ARB have been reported by the conventional SD-OCT,[4–6] however detailed structural changes of the photoreceptor layer had not been described. Instead, there are many studies that described the OCT features of the photoreceptor layer in eyes with VMD.[3,7–12] Augstburger et al. investigated the OCT images of different patients with VMD at different stages and reported on the characteristic OCT features of the outer retinal structures in different stages; the previtelliform stage with a slight foveal thickening of the interdigitation zone, the vitelliform stage with separation between the photoreceptor outer segments and RPE, the pseudohypopyon stage with the beginning of disintegration of the photoreceptor outer segments in the perifoveolar region, the vitelliruptive stage with severely reduced photoreceptor outer segment length and outer nuclear layer thickness, and the atrophic stage with completely disappeared subretinal fluid.[10]

Basically, our UHR-SD-OCT findings in patients with ARB did not contradict the previous findings in ARB and VMD as reported. However, due to the limited resolution of the conventional SD-OCT, the results of the previous studies did not show the disease-associated microstructures of the photoreceptors such as the string-of-pearls appearance with small HRDs of the outer segments (Fig. 3A, B and 3G, asterisks) and disrupted EZ which was composed of large HRDs (Fig. 3C and D, yellow arrowheads). Thus, our UHR-SD-OCT findings not only confirmed the earlier observations but also gave new insights about the possible pathological mechanism(s) involved in the retinal damages in the ARB.

The horizontal diameter of the large HRDs in the disrupted EZ was approximately 33 μm and that of the small HRDs in the outer segment were approximately 13 μm (Fig. 3). The size of small HRDs observed in the ARB was almost the same as that in OMD.[22] Because the horizontal diameter of HRDs was much larger than that of the normal cone inner segments in the paramacular regions (approx. 7 μm) or the cone outer segments at the fovea (approx. 1–2 μm),[28,29] both the HRDs in the disrupted EZ and outer segment observed in the UHR-SD-OCT images most likely do not represent individual photoreceptors but clusters of cone elements or abnormally expanded individual cone photoreceptors. The small HRDs in the outer segments may be packets of abnormal outer segment disks that changed their orientation in the process of phagocytosis, or they may be phagosomes being phagocytosed by the apical processes of the RPE just below the outer segment tips.[22,30,31] The abnormal phagocytosis of the outer segments during the disease process produced the cluster of rotated packets of outer segment disks which had abnormal hyperreflectivity in the outer segment region. The small HRDs may also be due to the increased reflectivity of the outer segments alone due to mechanical stress[32] or degenerative changes.[33] One possible source of the larger HRDs could be abnormal photoreceptor inner segment ellipsoids that have lost their connection with the normal outer segments. These ellipsoid particles may not contain normally functioning mitochondria and will lead to degeneration by apoptosis. The region with degenerated ellipsoids will lead to a further loss of nuclei and a thinning of ONL (Fig. 3E).

4.2. *Common and distinct features in cases with ARB and OMD*

In an earlier study with UHR-SD-OCT, we showed that during the early stages of OMD, the outer segments were hyperreflective with small HRDs aligned like icicles or string of pearls.[22] In addition, there was a disruption of the EZ which then appeared as clusters of larger HRDs[22] similar to the structural changes during the photoreceptor atrophy in ARB. However, the processes were distinctly different between the two diseases in other aspects. For example, the changes in the cone IZ and outer segments preceded that of the EZ in ARB, but the changes of the cone IZ, photoreceptor outer segments and EZ occurred simultaneously in OMD. Second, the EZ band completely disappeared in the later stage of ARB, but the EZ together with the outer segment space between the EZ and RPE were preserved in the later stages of OMD although the EZ was more blurred than in normal eyes. And third, the photoreceptor atrophy was followed by RPE disruption and inner retinal atrophy in ARB, but both the RPE and inner retinal structures were normally preserved in the later stages of OMD.

These differences can be explained by the pathological mechanisms of these diseases. In ARB, there is a dysfunction of the RPE leading to a

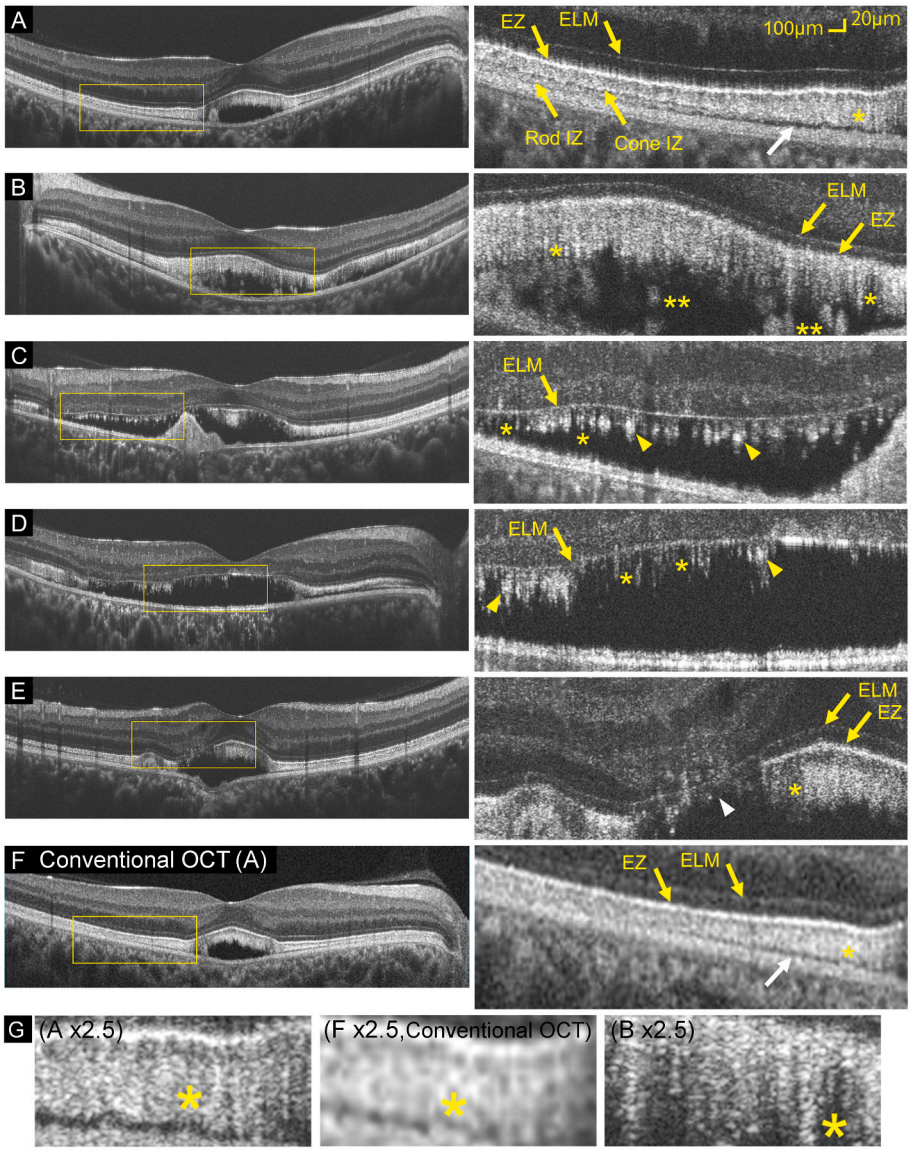

Fig. 3. B-scan images of five eyes in four cases with autosomal recessive bestrophinopathy (ARB), aligned according to the severity of the photoreceptor atrophy from mild to severe. **A.** Horizontal B-scan image of the right eye of a 33-year-old woman. In the expanded image, the EZ, cone IZ, and rod IZ are preserved in the peri-macular region (**yellow arrows**), but in the region with shallow retinal detachment, the cone IZ is absent (**white arrow**), and the outer segments is hyperreflective and elongated with small hyperreflective dots (HRDs) appearing like icicles or string of pearls hanging on the EZ (**asterisk**). **B.** Horizontal B-scan image of the left eye of a 20-year-old woman. In the expanded image, the outer segments are elongated with small HRDs appearing like icicles or string of pearls hanging on the EZ (**asterisks**). The peripheral edge of the outer segments is irregularly aligned and there are debris-like hyperreflective spots between the outer segments and the RPE (**double asterisks**). **C.** Vertical B-scan image of the left eye of a 36-year-old woman. In the expanded image, the outer segments are shortened and the EZ band is disrupted and composed of individual large HRDs (**yellow arrowheads**). These large HRDs are connected to the ELM with less highly reflective bridge-like structures, and part of the disrupted EZ appears thinner and hanging on the ELM (**asterisks**). **D.** Horizontal B-scan image of the right eye of a 55-year-old man. In the expanded image, an EZ-like band is not detected but a thin icicle-like structures can be seen hanging on the ELM (**yellow asterisks**) There are a small number of large HRDs hanging on the ELM at the location where EZ band should be in normal eyes (**yellow arrowheads**). **E.** Vertical B-scan image of the left eye of the patient in Fig. 3A. In the expanded image, the fovea shows preserved EZ and elongated outer segment with icicles-like structures (**yellow asterisk**). At the location of the disrupted EZ, the outer nuclear layer (ONL) is thin and the outer plexiform layer appears closer to the ELM (**white arrowhead**). There are hyperreflective spots scattered in the ONL above the disrupted EZ (**white arrowhead**) which are known as hyperreflective foci. **F. Conventional OCT.** Horizontal B-scan images of the same eye as in **A** taken by a conventional SD-OCT. In the expanded image, the ELM and EZ are observed (**yellow arrows**), but the cone IZ and rod IZ are not observed. There is a shallow retinal detachment in the parafoveal region (**white arrow**), but string-of-pearl like structure is not apparent. **G.** Further expanded images of the outer segment regions (asterisk) in the right column in **A**, **F**, and **B**. Left (**A x 2.5**, UHR-SD-OCT) and central (**F x 2.5**, Conventional OCT) images show the same region of the same eye for comparison. String-of-pearls appearance of the outer segment was apparent only in the UHR-SD-OCT images (left and right, **asterisks**). ELM = external limiting membrane; EZ = ellipsoid zone of photoreceptor; IZ = interdigitation zone of photoreceptor. (For interpretation of the references to colour in this figure legend, the reader is referred to the Web version of this article.)

defect in phagocytosis and secondary atrophy of the outer segments.[3,12,15,16] The mechanism causing the RPE abnormality in the *BEST1*-related retinal diseases is known to be related to the decreased function of Ca^{2+} dependent Cl^{-} channels at the basolateral plasma membrane of the RPE cells. The dysfunction of the RPE cells could explain both the abnormalities of the electrooculogram and the accumulation of lipofuscin, unphagocytosed photoreceptor outer segments, and SRF.[34,35] The toxicity of the accumulated lipofuscin and the long-standing mechanical separation of the outer segments from the RPE were suggested to induce the dysfunction and atrophy of the photoreceptor cells.

On the other hand, there is a dysfunction of the connecting cilia leading to atrophy of both the inner and outer segments of the photoreceptors in OMD.[36–38] Another difference is that both cone and rod photoreceptors are affected in ARB due to a generalized dysfunction of the RPE, whereas only the cone photoreceptors in the macular region are affected and rod photoreceptors are normally preserved until the late stages in OMD.[39] The preservation of the rod photoreceptors in OMD could partially explain the preserved EZ band and ONL thickness and normal RPE in the late stage which differs from the eyes with ARB.[22]

These suggestions are in accordance with the results of the observations of the UHR-SD-OCT images in cases of ARB that clearly indicated sequential changes in the outer retinal structures that were dependent on the severity of the photoreceptor atrophy. First, there is an increased reflectivity and presence of the small HRDs in the outer segments (Fig. 3A and G left). Then, there were irregularities and a decrease in the

length of the outer segments which leads to a complete loss of the outer segments (Fig. 3B and G right, and 3C). These changes were followed by the disruption of the EZ and the appearance of the large HRDs, *i.e.*, segmented ellipsoid regions, connected to the ELM (Fig. 3C and D). Then, there was a disappearance of the large HRDs and appearance of thin string-like icicles hanging directly from the ELM (Fig. 3D). Finally, there was a local thinning of the ONL and appearance of HRF above the disrupted EZ (Fig. 3E). These reflect very slowly progressive natural course in the *BEST1*-related maculopathies, and we assume that the serous SRF by itself may not be so harmful to the photoreceptor cells than the hyperreflective materials containing lipofuscin that were often observed in the early stage of VMD and ARB.

4.3. Limitations

Our study has several limitations. First, our study was retrospective and cross-sectional, and longitudinal changes were not observed in individual patients. Data of longitudinal follow-up examinations for individual patients will provide more precise information of the disease progression. Second, we selected patients with the same genetic abnormality because genotypic differences in the same gene may have different courses and severities in ARB.[5] However, to investigate the general mechanism of photoreceptor atrophy in more detail, data from a wider variety of genotypes and diseases of known etiology should be made.

In conclusion, the UHR-SD-OCT device can obtain images of the photoreceptor microstructures that show the structural changes in detail during the progression of ARB. The detailed observation will help clinicians and researchers to determine the mechanism of the retinal pathology and provide important information for the effectiveness of therapeutic strategies.

5. Patient consent

Consent to publish this case report has been obtained from the patients in writing. This report does not contain any personal identifying information.

Funding

This study was supported by research grants from the 'National Hospital Organization Network Research Fund (H30–NHO-Sensory Organs-03 to KT)' and 'Health and Labour Sciences Research Grant for research on intractable diseases from Ministry of Health, Labour and Welfare of Japan (20FC1057) to KT'.

The authors have no proprietary or commercial interest in any materials discussed in this article.

Authorship

All authors attest that they meet the current ICMJE criteria for Authorship.

Summary statement

Ultrahigh-resolution SD-OCT images revealed changes of the microstructures of the photoreceptors in eyes with autosomal recessive bestrophinopathy.

Author declaration

We wish to confirm that there are no known conflicts of interest associated with this publication and there has been no significant financial support for this work that could have influenced its outcome.

We confirm that the manuscript has been read and approved by all named authors and that there are no other persons who satisfied the criteria for authorship but are not listed. We further confirm that the order of authors listed in the manuscript has been approved by all of us.

We confirm that we have given due consideration to the protection of intellectual property associated with this work and that there are no impediments to publication, including the timing of publication, with respect to intellectual property. In so doing we confirm that we have followed the regulations of our institutions concerning intellectual property.

We further confirm that any aspect of the work covered in this manuscript that has involved human patients has been conducted with the ethical approval of all relevant bodies and that such approvals are acknowledged within the manuscript.

We understand that the Corresponding Author is the sole contact for the Editorial process (including Editorial Manager and direct communications with the office). He is responsible for communicating with the other authors about progress, submissions of revisions and final approval of proofs. We confirm that we have provided a current, correct email address which is accessible by the Corresponding Author.

Declaration of competing interest

K.T.: Payment for lectures - Santen Pharmaceutical Co., Ltd., Novartis Pharma Co., Ltd., Kowa Company, Ltd., and Senju Pharmaceutical Co.,Ltd. Receipt of equipment - Kowa Company, Ltd.

G.H.: None.

The funding sources had no role in the design and conduct of this study; collection, management, analysis, interpretation of the data; preparation, review, or approval of the manuscript; and decision to submit the manuscript for publication.

Acknowledgements

We thank all the subjects for participation in this study. We thank Masaharu Mizouchi of Kowa Company for technical support. We thank our collaborators, Takeshi Iwata, Kaoru Fujinami and Natsuko Nakamura of the National Institute of Sensory Organs for their contributions in genetic analysis of the patients. We also thank Professor Emeritus Duco Hamasaki of the Bascom Palmer Eye Institute, University of Miami School of Medicine, Miami, FL for discussions and editing our manuscript.

Appendix A. Supplementary data

Supplementary data to this article can be found online at https://doi.org/10.1016/j.ajoc.2022.101706.

References

1. Schatz P, Klar J, Andréasson S, Ponjavic V, Dahl N. Variant phenotype of Best vitelliform macular dystrophy associated with compound heterozygous mutations in VMD2. *Ophthalmic Genet.* 2006;27:51–56.
2. Burgess R, Millar ID, Leroy BP, et al. Biallelic mutation of BEST1 causes a distinct retinopathy in humans. *Am J Hum Genet.* 2008;82:19–31.
3. Boon CJ, Klevering BJ, Leroy BP, Hoyng CB, Keunen JE, den Hollander AI. The spectrum of ocular phenotypes caused by mutations in the BEST1 gene. *Prog Retin Eye Res.* 2009;28:187–205.
4. Nakanishi A, Ueno S, Hayashi T, et al. Clinical and genetic findings of autosomal recessive bestrophinopathy in Japanese cohort. *Am J Ophthalmol.* 2016;168:86–94.
5. Casalino G, Khan KN, Armengol M, et al. Autosomal recessive bestrophinopathy: clinical features, natural history, and genetic findings in preparation for clinical trials. *Ophthalmology.* 2021;128:706–718.
6. Pfister TA, Zein WM, Cukras CA, et al. Phenotypic and genetic spectrum of autosomal recessive bestrophinopathy and best vitelliform macular dystrophy. *Invest Ophthalmol Vis Sci.* 2021;62:22.
7. Kay CN, Abramoff MD, Mullins RF, et al. Three-dimensional distribution of the vitelliform lesion, photoreceptors, and retinal pigment epithelium in the macula of patients with best vitelliform macular dystrophy. *Arch Ophthalmol.* 2012;130:357–364.
8. Kay DB, Land ME, Cooper RF, et al. Outer retinal structure in best vitelliform macular dystrophy. *JAMA ophthalmol.* 2013;131:1207–1215.

9. Chen KC, Jung JJ, Curcio CA, et al. Intraretinal hyperreflective foci in acquired vitelliform lesions of the macula: clinical and histologic study. *Am J Ophthalmol*. 2016;164:89–98.
10. Augstburger E, Orès R, Mohand-Said S, et al. Outer retinal alterations associated with visual outcomes in best vitelliform macular dystrophy. *Am J Ophthalmol*. 2019; 208:429–437.
11. Lima de Carvalho Jr JR, Paavo M, Chen L, Chiang J, Tsang SH, Sparrow JR. Multimodal imaging in best vitelliform macular dystrophy. *Invest Ophthalmol Vis Sci*. 2019;60:2012–2022.
12. Qian CX, Charran D, Strong CR, Steffens TJ, Jayasundera T, Heckenlively JR. Optical coherence tomography examination of the retinal pigment epithelium in best vitelliform macular dystrophy. *Ophthalmology*. 2017;124:456–463.
13. Weingeist TA, Kobrin JL, Watzke RC. Histopathology of Best's macular dystrophy. *Arch Ophthalmol*. 1982;100:1108–1114.
14. O'Gorman S, Flaherty WA, Fishman GA, Berson EL. Histopathologic findings in Best's vitelliform macular dystrophy. *Arch Ophthalmol*. 1988;106:1261–1268.
15. Mullins RF, Oh KT, Heffron E, Hageman GS, Stone EM. Late development of vitelliform lesions and flecks in a patient with best disease: clinicopathologic correlation. *Arch Ophthalmol*. 2005;123:1588–1594.
16. Mullins RF, Kuehn MH, Faidley EA, Syed NA, Stone EM. Differential macular and peripheral expression of bestrophin in human eyes and its implication for best disease. *Invest Ophthalmol Vis Sci*. 2007;48:3372–3380.
17. Zhang Q, Small KW, Grossniklaus HE. Clinicopathologic findings in Best vitelliform macular dystrophy. In: *Graefe's archive for clinical and experimental ophthalmology = Albrecht von Graefes Archiv fur klinische und experimentelle Ophthalmologie*. 249. 2011: 745–751.
18. Matsui Y, Kondo M, Uchiyama E, Mityata R, Matsubara H. New clinical ultrahigh-resolution SD-OCT using A-scan matching algorithm. In: *Graefe's archive for clinical and experimental ophthalmology = Albrecht von Graefes Archiv fur klinische und experimentelle Ophthalmologie*. 257. 2019:255–263.
19. Matsui Y, Miyata R, Uchiyama E, Matsubara H, Kondo M. Misalignment of foveal pit and foveal bulge determined by ultrahigh-resolution SD-OCT in normal eyes. Graefe's archive for clinical and experimental ophthalmology. In: = *Albrecht von Graefes Archiv fur klinische und experimentelle Ophthalmologie*. 258. 2020:2131–2139.
20. Cideciyan AV, Jacobson SG. Leber congenital amaurosis (LCA): potential for improvement of vision. *Invest Ophthalmol Vis Sci*. 2019;60:1680–1695.
21. Peshenko IV, Cideciyan AV, Sumaroka A, et al. A G86R mutation in the calcium-sensor protein GCAP1 alters regulation of retinal guanylyl cyclase and causes dominant cone-rod degeneration. *J Biol Chem*. 2019;294:3476–3488.
22. Tsunoda K, Hanazono G. Detailed analyses of microstructure of photoreceptor layer at different severities of occult macular dystrophy by ultrahigh-resolution SD-OCT. *Am. j. ophthalmol. case rep.* 2022;26, 101490.
23. McCulloch DL, Marmor MF, Brigell MG, et al. ISCEV Standard for full-field clinical electroretinography (2015 update). *Doc Ophthalmol*. 2015;130:1–12.
24. Kameya S, Fujinami K, Ueno S, et al. Phenotypical characteristics of POC1B-associated retinopathy in Japanese cohort: cone dystrophy with normal funduscopic appearance. *Invest Ophthalmol Vis Sci*. 2019;60:3432–3446.
25. Tian R, Yang G, Wang J, Chen Y. Screening for BEST1 gene mutations in Chinese patients with bestrophinopathy. *Mol Vis*. 2014;20:1594–1604.
26. Staurenghi G, Sadda S, Chakravarthy U, Spaide RF. Proposed lexicon for anatomic landmarks in normal posterior segment spectral-domain optical coherence tomography: the IN*OCT consensus. *Ophthalmology*. 2014;121:1572–1578.
27. Parodi MB, Romano F, Sacconi R, et al. Intraretinal hyperreflective FOCI IN best vitelliform macular dystrophy. *Retina*. 2018;38:2379–2386.
28. Curcio CA, Sloan KR, Kalina RE, Hendrickson AE. Human photoreceptor topography. *J Comp Neurol*. 1990;292:497–523.
29. Liu J, Jung H, Dubra A, Tam J. Cone photoreceptor cell segmentation and diameter measurement on adaptive optics images using circularly constrained active contour model. *Invest Ophthalmol Vis Sci*. 2018;59:4639–4652.
30. Steinberg RH, Wood I, Hogan MJ. Pigment epithelial ensheathment and phagocytosis of extrafoveal cones in human retina. *Philos Trans R Soc Lond Ser B Biol Sci*. 1977;277:459–474.
31. Anderson DH, Fisher SK, Steinberg RH. Mammalian cones: disc shedding, phagocytosis, and renewal. *Invest Ophthalmol Vis Sci*. 1978;17:117–133.
32. Scharf JM, Hilely A, Preti RC, et al. Hyperreflective stress lines and macular holes. *Invest Ophthalmol Vis Sci*. 2020;61:50.
33. Nagasaka Y, Ito Y, Ueno S, Terasaki H. Number of hyperreflective foci in the outer retina correlates with inflammation and photoreceptor degeneration in retinitis pigmentosa. *Ophthalmol. Retina*. 2018;2:726–734.
34. Sun H, Tsunenari T, Yau KW, Nathans J. The vitelliform macular dystrophy protein defines a new family of chloride channels. *Proc Natl Acad Sci U S A*. 2002;99: 4008–4013.
35. Hartzell HC, Qu Z, Yu K, Xiao Q, Chien LT. Molecular physiology of bestrophins: multifunctional membrane proteins linked to best disease and other retinopathies. *Physiol Rev*. 2008;88:639–672.
36. Conte I, Lestingi M, den Hollander A, et al. Identification and characterisation of the retinitis pigmentosa 1-like1 gene (RP1L1): a novel candidate for retinal degenerations. *Eur J Hum Genet : EJHG (Eur J Hum Genet)*. 2003;11:155–162.
37. Akahori M, Tsunoda K, Miyake Y, et al. Dominant mutations in RP1L1 are responsible for occult macular dystrophy. *Am J Hum Genet*. 2010;87:424–429.
38. Yamashita T, Liu J, Gao J, et al. Essential and synergistic roles of RP1 and RP1L1 in rod photoreceptor axoneme and retinitis pigmentosa. *J Neurosci*. 2009;29: 9748–9760.
39. Miyake Y, Horiguchi M, Tomita N, et al. Occult macular dystrophy. *Am J Ophthalmol*. 1996;122:644–653.